Steps towards a Reynolds Stress Model for the Prediction of Separated Flows

Bernhard Eisfeld
DLR, Institute of Aerodynamics and Flow Technology
Lilienthalplatz 7, D-38108 Braunschweig
GERMANY

bernhard.eisfeld@dlr.de

ABSTRACT

A tailored strategy based on Reynolds stress modelling is suggested for improving the prediction of separated flows. The strategy is based on the observation that the turbulence structure differs between different flows. A full description of the turbulence structure requires the full information about the Reynolds-stress anisotropies rather than the invariants alone. Success of the strategy is demonstrated by applying a zonally modified Reynolds stress model for improved prediction of a plane mixing layer to separating flows, leading to shorter separation bubbles. Combination with a recently developed length-scale correction maintains the pressure distribution, but moves the reattachment point downstream again.

NOMENCLATURE

Latin symbols

Symbol	Units	Meaning
b_{ij}	1	Component of Reynolds stress anisotropy tensor
c	m	Chord length
c_f	1	Local skin friction coefficient
C_p	1	Pressure coefficient
F_1	1	Blending function by Menter [2]
H	m	Step height
I_b	1	First invariant of Reynolds stress anisotropy tensor (= trace)
II_b	1	Second invariant of Reynolds stress anisotropy tensor
III_b	1	Third invariant of Reynolds stress anisotropy tensor (= determinant)
$\tilde{k}$	m^2/s^2	Specific kinetic turbulence energy
N	1	Number of grid points or cells
$\tilde{R}_{ij}$	m^2/s^2	Specific Reynolds stress (tensor component)
Re_L	1	Reynolds number based on reference length L

u_i''	m/s	Component of fluctuating velocity

Greek symbols

Symbol	Units	Meaning
δ_{ij}	1	Kronecker symbol
θ	rad	Inclination angle of Reynolds stress principle axis system
$\lambda_i^{(A)}$		Eigenvalue of tensor $\boldsymbol{A}$
$\bar{\rho}$	kg/m^3	Mean fluid density

1.0 INTRODUCTION

The prediction of smooth-wall separation is one of the most demanding challenges in Computational Fluid Dynamics (CFD). Based on the Reynolds-averaged Navier-Stokes (RANS) equations, eddy viscosity models (EVM) have been developed like the Spalart-Allmaras [1] model or the Shear-Stress Transport model (SST) by Menter [2] that currently set the standards for CFD applications in aeronautics. They are numerically well behaved and show a high degree of reliability for attached flows. Nevertheless, with separating flows their predictive accuracy degrades.

Improvement might be expected from scale-resolving methods like Large-Eddy Simulations (LES) or hybrid RANS/LES methods, e.g. Delayed Detached Eddy Simulation (DDES) [3]. However, time-dependent scale-resolution considerably increases the numerical effort compared to standard RANS methods. Furthermore, in particular with smooth-wall separation, large portions of the flow field are still governed by attached boundary layers showing little large-scale unsteadiness. Hence, any improvement of RANS models for predicting at least mild separation would be highly welcome.

A possible strategy for improvement might be replacing the models based on the phenomenological eddy-viscosity assumption by a model based on the known transport equations for the individual components of the Reynolds-stress tensor and an additional transport equation for a length-scale providing variable. With such so-called Reynolds-stress model (RSM) the production of turbulence is given exactly, e.g. giving rise to free vortices being predicted more compact and in closer agreement with experiments than predicted with EVM that require additional rotational corrections. Furthermore the individual treatment of Reynolds stresses allows for reflecting the so-called normal-stress anisotropy near walls that is ignored by the Boussinesq hypothesis, which is the basis for linear EVM. Generally, the RSM approach allows for calibrating according to the different Reynolds stresses, whereas with linear EVM, calibration is limited to one component of the Reynolds-stress tensor only, usually the shear stress. For extending the degrees of freedom of EVM-calibration, non-linear extensions are required, e.g. [4], increasing the demand for grid resolution.

In the past, the SSG/LRR-ω Reynolds stress model has been developed [5][6], showing promising results for a variety of flows [7]. Nevertheless, this model has not been particularly tuned for predicting smooth-wall separation and, therefore, still requires improvement. First steps have been made in this direction, involving

fundamental considerations as well as empirical observations.

Only recently it has been shown that the turbulence structure differs even between simple canonical free-shear flows [8], requiring an individual treatment of different flow situations. In particular, it has been demonstrated that predictions of a plane mixing layer can be improved, when calibrating an RSM accordingly [8]. Because of its relation to the shear layer above a recirculation region, such treatment is supposed to transfer to separating flows. Additionally, an empirical length-scale correction has been developed for the SSG/LRR-ω model, improving the behavior of separated flows particularly near reattachment [9].

After recalling the foundations of characterizing the turbulence structure and its difference between different flows, the above modifications are applied to separating flows, confirming the baseline considerations of tailored modeling.

2.0 TURBULENCE STRUCTURE

2.1 Fundamental Considerations

Within the compressible RANS equations, the net effect of the turbulent motion on the mean momentum is described by the Reynolds stresses $\bar{\rho}\tilde{R}_{ij} = \overline{\rho u_i'' u_j''}$, where ρ denotes the density, u_i'' a fluctuating velocity component with respect to the mass-weighted average and the overbar indicates an averaging operation. The Reynolds stresses represent components of a symmetric tensor that, hence, has three real eigenvalues $\lambda_i^{(R)} \geq 0$, associated with an ellipsoid with semi-axes of length $\sqrt{\lambda_i^{(R)}}$.

For analysing the structure of turbulence, a non-dimensional anisotropy tensor $\boldsymbol{b}$ is defined with components

$$b_{ij} = \frac{\tilde{R}_{ij}}{2\tilde{k}} - \frac{1}{3}\delta_{ij} \tag{1}$$

in which δ_{ij} represents the Kronecker symbol and $\tilde{k} = \frac{1}{2}\tilde{R}_{kk}$ is the specific kinetic turbulence energy. The anisotropy tensor is symmetric, $b_{ij} = b_{ji}$, and traceless, $b_{ii} = 0$ (summation on i). Its eigenvalues follow from the characteristic equation

$$-\left(\lambda^{(b)}\right)^3 + I_b\left(\lambda^{(b)}\right)^2 - II_b\lambda^{(b)} + III_b = 0, \tag{2}$$

in which

$$I_b = b_{ii} = \lambda_1^{(b)} + \lambda_2^{(b)} + \lambda_3^{(b)} = 0, \tag{3}$$

$$II_b = -\frac{1}{2}b_{ij}b_{ji} = \lambda_1^{(b)}\lambda_2^{(b)} + \lambda_2^{(b)}\lambda_3^{(b)} + \lambda_3^{(b)}\lambda_1^{(b)}, \tag{4}$$

$$III_b = \frac{1}{3}b_{ij}b_{jk}b_{ki} = \lambda_1^{(b)}\lambda_2^{(b)}\lambda_3^{(b)} \tag{5}$$

are the invariants of the anisotropy tensor that are closely related to its eigenvalues. The structure of turbulence is typically characterised in terms of the non-zero invariants II_b and III_b [10], whereas the mathematical properties of a tensor are usually analysed in terms of its eigenvalues. They define the ratio of the semi-axes and, thus, the shape of the ellipsoid associated with the Reynolds-stress tensor.

However, the physics of flow is governed by the transfer of mean momentum normal to the mean-flow

direction characterised by the corresponding Reynolds-shear stress and its anisotropy. For planar flow, the shear-stress component of the anisotropy tensor can be computed from the eigenvalues associated with the flow plane according to [8]

$$b_{12} = \left(\lambda_1^{(b)} - \lambda_2^{(b)}\right) \sin\theta \cos\theta, \tag{9}$$

in which θ is the inclination angle of the principle-axis system of the anisotropy tensor against the flow-aligned reference frame. Clearly, the shear-stress component vanishes for rotation angles of $\theta = n\frac{\pi}{2}$ and reaches its extreme values at $\theta = \frac{\pi}{4} + n\frac{\pi}{2}$, in which $n = 0, \pm 1, \pm 2, \ldots$

Moreover, for non-zero shear-stress anisotropy the eigenvalues $\lambda_1^{(b)}$ and $\lambda_2^{(b)}$ need to be different, i.e. the Reynolds-stress tensor must not be isotropic, at least in the plane considered. The largest difference of the eigenvalues is achieved in one-component turbulence, where $\lambda_1^{(b)} = \lambda_{max}^{(b)} = \frac{2}{3}$ and $\lambda_2^{(b)} = \lambda_{min}^{(b)} = -\frac{1}{3}$, whereas the typical assumptions for boundary layers are associated with eigenvalues $\lambda_1^{(b)} = -\lambda_2^{(b)} = 0.187$ [8].

Figure 9-1 shows the Reynolds-shear-stress anisotropy observed in a reference frame typically aligned with the main-flow direction, versus the inclination angle of the principal axis system of the anisotropy tensor against this reference frame. For comparison, the curves for the extreme conditions of one-component turbulence and for typical boundary-layer conditions are plotted. As one can see, the possible maximum and minimum values depend on the specific flow conditions, i.e. the eigenvalues $\lambda_1^{(b)}$ and $\lambda_2^{(b)}$. Nevertheless, any value of the Reynolds-shear-stress anisotropy in the range

$$-\frac{1}{2}\left|\lambda_1^{(b)} - \lambda_2^{(b)}\right| \leq b_{12} \leq +\frac{1}{2}\left|\lambda_1^{(b)} - \lambda_2^{(b)}\right|$$

can be achieved for given eigenvalues $\lambda_1^{(b)}$, $\lambda_2^{(b)}$ or invariants II_b, III_b, respectively, depending on the orientation of the principal axes of the Reynolds-stress (anisotropy) tensor.

Based on these fundamental considerations it must be concluded that, for a correct prediction of lateral mean-momentum transfer, the orientation of the principal axis system of the Reynolds-stress (anisotropy) tensor is of utmost importance. Therefore, improved predictions require accounting for the full information contained in the anisotropy tensor in advanced turbulence modelling [8], e.g. by a respective calibration. Considering the invariants only will not be sufficient.

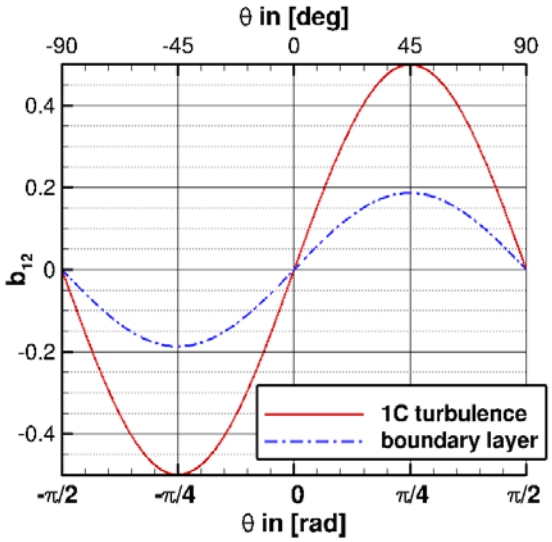

Figure 9-1: Reynolds-shear-stress anisotropy vs. inclination angle of principal axis system of the anisotropy tensor.

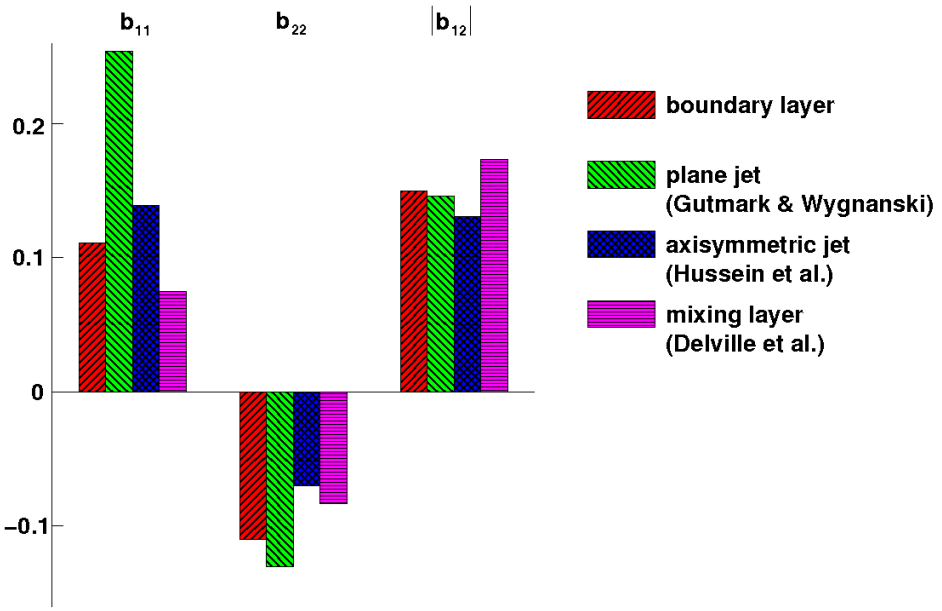

Figure 9-2: Constant Reynolds-stress anisotropy components in different shear flows.

2.2 Turbulent Shear Flows

Recently, based on theoretical considerations, a layer of constant anisotropy has been identified near the position of maximum Reynolds-shear stress [8] in experimental data for the plane jet [11], the axisymmetric jet [12] and the plane mixing layer [13]. Figure 9-2 shows a comparison of the anisotropy components found in the respective constant layer of the different flows, where the boundary layer values refer to the standard assumptions $b_{11} = -b_{22} = 0.111$ and $b_{12} = -0.15$.

Obviously, there exist considerable differences between the different flows, mainly in the normal-stress

components b_{11} and b_{22}. Nevertheless, comparing the boundary layer and the plane mixing layer, the invariants appear to be very similar [8], whereas the absolute values of the shear-stress anisotropy $|b_{12}|$ differ, indicating different lateral mean-momentum transfer.

Accurate predictions require reflecting these differences in turbulence structure between the different types of flows by an advanced turbulence model.

2.3 Turbulence Modelling Strategy

The difference observed in the absolute values of the shear-stress anisotropy $|b_{12}|$ can be associated with well-known deficiencies of RANS turbulence models. Such models are typically calibrated for turbulent equilibrium conditions, assuming a representative value for the shear-stress anisotropy, usually, according to the Bradshaw hypothesis [14], $b_{12} = -0.15$ for boundary layers. Obviously, this procedure is in contradiction to the above experimental observations, since it implies identical lateral transport of mean-flow momentum.

Indeed, according to Wilcox [15], there exists the so-called round-jet/plane-jet anomaly, stating that, without modification, RANS models predict the spreading rate of the axisymmetric jet larger than that of the plane jet, whereas experimentally the opposite is observed. This is in line with $|b_{12}| < 0.15$ in an axisymmetric jet.

It is also observed that RANS-models that are sensitive to separation, often predict reattachment too far downstream compared to experimental data due to an underestimation of the Reynolds-shear stress component in the shear layer above the separation bubble [16]. This shear layer, however, is related to the plane mixing layer [17]. Hence, the stated model deficiency is in line with the experimental finding of $|b_{12}| > 0.15$ in the plane mixing layer.

The observed differences in turbulence structure in conjunction with the known model deficiencies suggest that any turbulence model consisting of a fixed set of terms with fixed parameters and closure coefficients will never be able to predict different types of flow to an equal degree of accuracy. In particular, a calibration according to the characteristics of an attached boundary layer is in contradiction to the characteristics of a separating shear layer.

For improvement, an adaptive modelling approach will be required, providing tailored formulations, depending on the local type of flow. For this purpose, Reynolds-stress models appear particularly suited because they allow for a calibration according to the turbulence structure in the constant-anisotropy layer. In contrast, eddy-viscosity models will always predict the principal axis system of the Reynolds-stress tensor being rotated by $\theta = \pm\frac{\pi}{2}$ against the mean-flow direction of characteristic shear layers [8].

3.0 PROOF OF CONCEPT

The SSG/LRR-ω model [5][6] provides a suitable framework for testing the concept of tailoring because it already distinguishes a near-wall layer (LRR) from the rest of the flow field (SSG), where Menter's F_1-blending function [2] is used for switching. Recently, it has been demonstrated that recalibrating the SSG-part according to the anisotropies in a plane mixing layer shown in Fig. 9-2, indeed yields improved agreement with the experimental data by Delville et al. [13] for the Reynolds-shear stress in the plane mixing layer [8].

This modified model serves as simple prototype of a tailored model according to the above considerations. Because of the close relation between the plane mixing layer and the shear layer above a recirculation zone, it is subsequently applied to flows involving separation for proving the concept of tailoring.

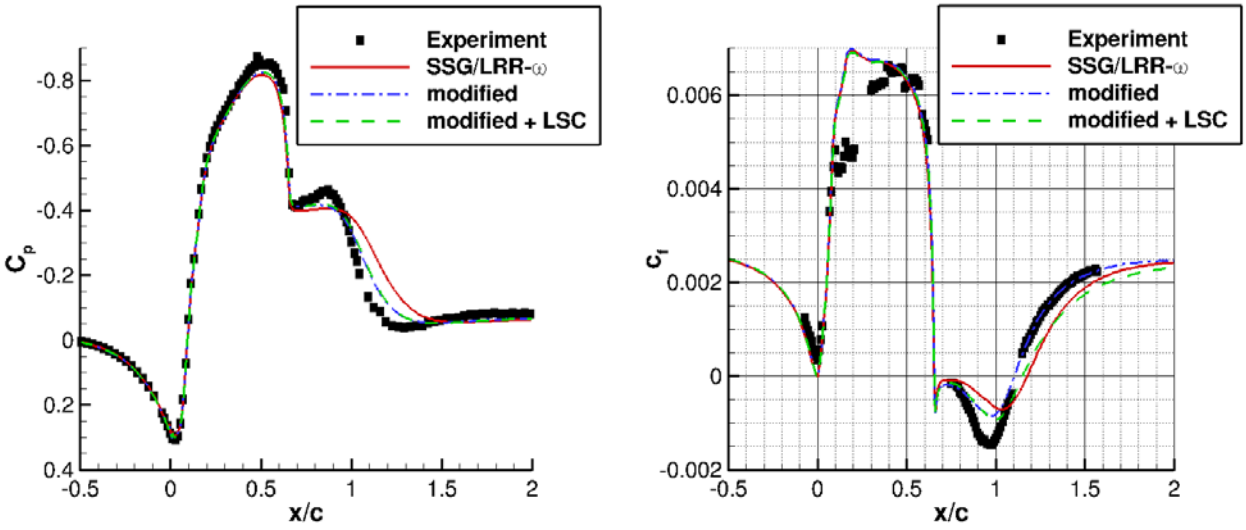

Figure 9-3: NASA-hump flow. Pressure coefficient (left) and skin-friction coefficient (right). Comparison of SSG/LRR-ω model with modified model recalibrated for plane mixing layer anisotropies and additional length-scale correction (LSC).

3.1 NASA-hump

The flow over the so-called NASA-hump [18][19][20] exhibits a rapid increase in pressure downstream of the hump's crest, leading to separation of the flow. Computations have been carried out with DLR's unstructured flow solver TAU [21], using the second-finest grid provided on NASA's Turbulence Modeling Resource (TMR) website [22] consisting of $N = 176{,}256$ cells. The Reynolds number based on the chord length c of the hump is $Re_c = 936{,}000$.

Figure 9-3 shows the distributions of the pressure coefficient C_p (left) and the skin friction coefficient c_f (right) obtained with the modified model compared to results by the original SSG/LRR-ω model and experimental data. Clearly, the modification improves the predictions in terms of the pressure recovery and the increase in skin friction downstream of the reattachment point. Compared to the original model, the modification leads to a shorter recirculation zone, where the predicted location of the reattachment point is in very good agreement with the experimental location at $x/c = 1.1$.

3.2 Backward-Facing Step

The flow over a backward-facing step [23] is used for assessing turbulence models with respect to predicting the reattachment location. Computations have been carried with TAU on the second finest grid provided on the TMR website [22], consisting of $N = 319{,}468$ cells. The Reynolds number based on the step height H is $Re_H = 36{,}000$.

Figure 9-4 shows the distributions of the pressure coefficient C_p (left) and the skin friction coefficient c_f (right) obtained with the modified model compared to results by the original SSG/LRR-ω model and experimental data. Some improvement is obtained with respect to the pressure recovery downstream of the separation. As with the NASA-hump, this is accompanied by an upstream shift of the reattachment point, which in this case, however, degrades the agreement with the experimental data.

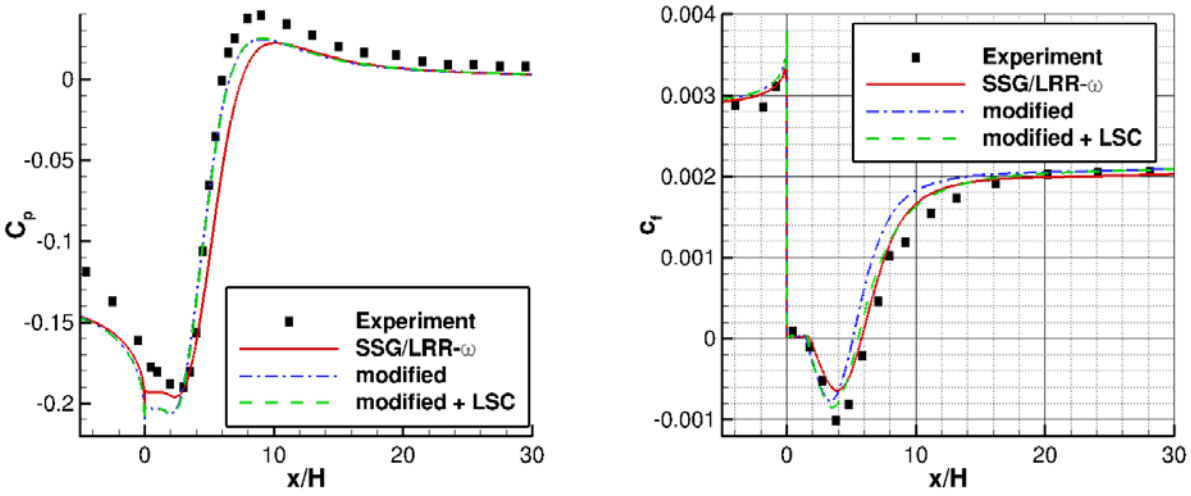

Figure 9-4: Flow over a backward-facing step. Pressure coefficient (left) and skin-friction coefficient (right). Comparison of SSG/LRR-ω model with modified model recalibrated for plane mixing layer anisotropies and additional length-scale correction (LSC).

3.3 Analysis of Results

Comparing the results for the flow over the NASA-hump and for the flow over the backward-facing step, the same effect is observed. Recalibrating the SSG-part of the model according to the anisotropy data by Delville et al. [13] for the plane mixing layer reduces the predicted separation length and enhances reattachment. Recall that the absolute value of the corresponding shear-stress anisotropy is higher than the standard value for boundary layers according to the Bradshaw hypothesis [14].

Figure 9-5 shows the streamline patterns of both flows together with contours of Menter's F_1-function [24] used for blending between the different parts of the modified model. Regions in blue indicate where the modified SSG-part is active, whereas regions in red refer to regions where the unmodified LRR-part is active. Indeed, in both flows the reattaching streamline is passing through an area, where the modified SSG-part is active, explaining why the modification influences the location of the reattachment point.

The results confirm the relation between the Reynolds-shear stress in the shear layer above a circulation bubble and its length, which is often overestimated [16]. The local modification according to the characteristics of a plane mixing layer indeed reduces the predicted bubble length, supporting the concept of tailored modelling.

Nevertheless, general improvement compared to experimental data is achieved only for the NASA-hump, whereas for the backward-facing step the bubble-length is underestimated. While this inconsistency of results is generally observed with RANS models [22], its origin is still unknown. One possible influence could be due to the modelled turbulent length scale, which is investigated in the next section.

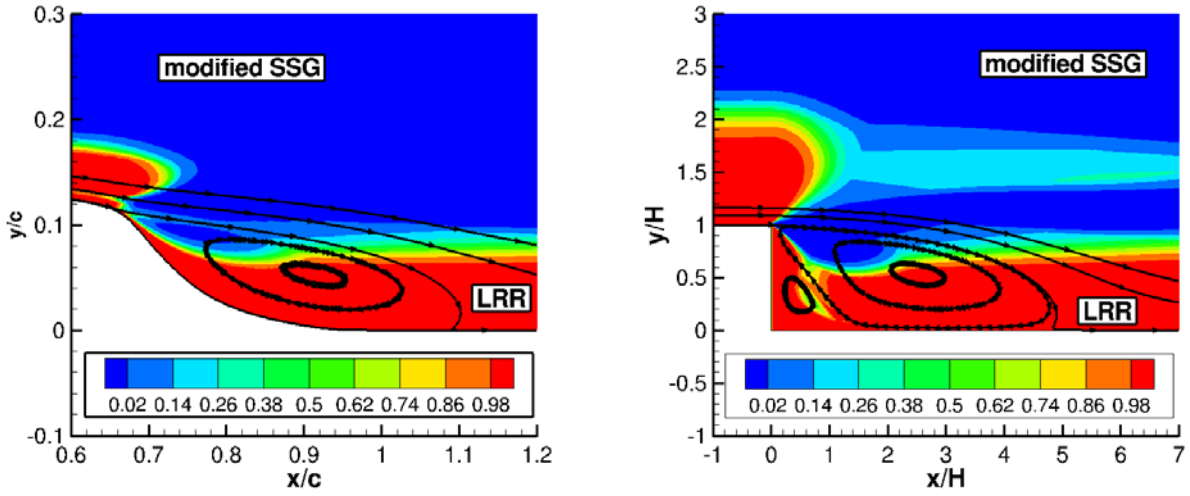

Figure 9-5: Flow over the NASA-hump (left) and over a backward-facing step (right). Streamline patterns for modified RSM. Contours of blending function F_1 indicate the regions, where the modified SSG-part (blue) and the unmodified LRR-part of the model (red) are active.

4.0 LENGTH SCALE

With Reynolds-stress models, the reattaching streamline typically shows an unphysical back-bending that is also present in Fig. 9-5. It can be associated with a deficiency in the length-scale equation [25] that can be removed by a length-scale correction (LSC) that has been developed recently for the SSG/LRR-ω model [9]. Based on an analysis of the so-called Yap correction [26][27], the ω-destruction term is switched-off in near-wall regions, where an excessive turbulent length-scale is detected. This modification not only remedies the unphysical back-bending of the reattaching streamline but also shifts the reattachment point further downstream, often in better agreement with experimental data than the baseline SSG/LRR-ω model [9].

Obviously, the LSC has the opposite effect on the reattachment location than the above modification according to the plane mixing layer characteristics. Therefore, it is interesting to study a possible compensation of effects that may influence the observed inconsistency of the results for the NASA-hump and the back-ward-facing step.

For this purpose, the LSC has been combined with the modified model, employing the recalibrated SSG-part, and has been applied to the two test cases. The corresponding results have been included in Figs. 9-3 and 9-4.

Similar to what has been previously observed [9], the pressure distributions remain virtually unaffected i.e., the improvement in C_p obtained by recalibrating the SSG-part according to the anisotropies of the plane mixing layer is maintained. In contrast, but as expected according to previous observations [9], the LSC moves the respective reattachment point downstream so that it is in fact predicted close to the location predicted by the original SSG/LRR-ω model. Thus, the compensating effects of both model modifications do not remedy the inconsistency between the predictions for the NASA-hump and the backward-facing step, leaving the reasons still an open question.

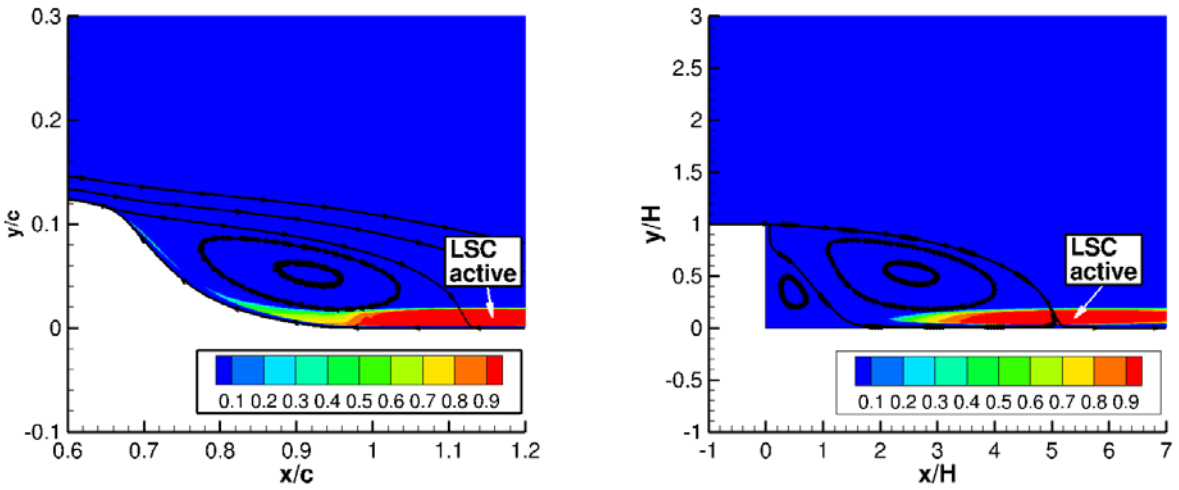

Figure 9-6: Flow over the NASA-hump (left) and over a backward-facing step (right). Streamline patterns for modified RSM with additional length-scale correction. Contours of length-scale correction $F^{(LSC)}$ indicate the regions, where the length-scale correction (LSC) is active (red).

Figure 9-6 shows the streamline patterns predicted by the modified model with the additional length-scale correction for the flow over the NASA-hump (left) and the flow over the backward-facing step (right). Comparison with Fig. 9-5 shows that the back-bending of the reattaching streamline indeed is remedied. Note that the normal coordinate is stretched compared to the stream wise coordinate. Hence the effect is even larger than it appears.

The colours in Fig 9-6 indicate where the LSC is active. Clearly, its activity is limited to a region near the wall, resembling the results obtained for the original SSG/LRR-ω model [9]. Comparison with Fig. 9-5 reveals that the LSC is active only in the region, where also the unaltered LRR-part of the model is active, explaining the similarity of the observations.

5.0 CONCLUSION

The structure of turbulence is characterised by the invariants of the Reynolds-stress anisotropy tensor together with the orientation of its principal axes. In particular, in planar flow, the Reynolds-shear stress depends on the inclination of the principal axes against the flow-aligned coordinate system.

A previous analysis has revealed a layer of constant anisotropies in different free-shear flows, showing differences in the turbulence structure between the different types of flow. These differences need to be accounted for by advanced turbulence models, suggesting a tailored modelling strategy.

In order to prove this concept, a modified SSG/LRR-ω Reynolds-stress model, in which the SSG-part has previously been recalibrated to the anisotropies in a plane mixing layer [8], has been used as a prototype and applied to the flow over the NASA-hump and a backward-facing step. The simulation results show that the reattaching streamlines are passing a region, where the modification is active, which is accompanied by an upstream shift of the reattachment point. This confirms the observation that the Reynolds-shear stress in the shear layer above the recirculation zone determines the location of reattachment.

Without modification, the reattaching streamlines show an unphysical back-bending that has recently been

remedied by a length-scale correction for the SSG/LRR-ω model [9]. In the present study, this length-scale correction has been added to the modified RSM with the recalibrated SSG-part. Similar to previous observations, this has almost no effect on the pressure distribution, while the reattachment point is moved downstream again.

The known inconsistency between the results for the NASA-hump and the backward-facing step are not remedied by the opposite effects of both modifications. Additional highly reliable experimental data seem to be required for providing a deeper understanding of the differences between the two flows.

Nevertheless, the results obtained support a tailored modelling strategy based on RSM, accounting for differences in turbulence structure between different types of flow. Future development is aiming at a self-adaptive model, requiring suitable indicators for more precisely identifying the respective type of flow. In particular, detection of separated shear layers should be more precise than in the approach presented. Furthermore, the range of characteristic flow types to be detected needs to be extended, e.g. to jet and wake flows.

REFERENCES

[1] Spalart, P.R., Allmaras, S.R.: A one-equation turbulence model for aerodynamic flows, La Recherche Aérospatiale, Vol 1, 1994, pp. 5-21.

[2] Menter, F.R.: Two-Equation Eddy-Viscosity Turbulence Models for Engineering Applications, AIAA Journal, Vol. 32 No. 8, 1994, pp. 1598-1605.

[3] Spalart, P.R., Deck, S., Shur, M.L., Squires, K.D., Strelets, M. Kh., Travin, A.: A New Version of Detached-eddy Simulation, Resistant to Ambiguous Grid Densities, Theoretical and Computational Fluid Dynamics, Vol. 20 No. 3, 2006, pp.181-195.

[4] Spalart, P. R.:Strategies for Turbulence Modelling and Simulation, International Journal of Heat and Fluid Flow, Vol. 21, 2000, pp. 252-263.

[5] Eisfeld, B., Brodersen, O.: Advanced Turbulence Modeling and Stress Analysis for the DLR-F6 Configuration, AIAA-Paper 2005-4727, 2005.

[6] Cecora, R.-D., Radespiel, R., Eisfeld, B., Probst, A.: Differential Reynolds-Stress Modeling for Aeronautics, AIAA Journal, Vol. 53 No. 3, 2015, pp. 739-755.

[7] Eisfeld, B., Rumsey, C., Togiti, V.: Verification and Validation of a Second-Moment-Closure Model, AIAA Journal, Vol. 54 No. 5, 2016, pp. 1524-1541.

[8] Eisfeld, B.; Turbulence Modeling for Free Shear Flows, AIAA-Paper 2019-2962. 2019.

[9] Eisfeld, B., Rumsey, C.: Length-Scale Correction for Reynolds Stress Modeling, AIAA-Paper 2019-2961, 2019.

[10] Lumley, J.L.: Computational Modeling of Turbulent Flows, Adv. Appl. Mech., Vol. 18, 1978, pp- 123-176.

[11] Gutmark, E., Wygnanski, I.: The planar turbulent jet, Journal of Fluid Mechanics, Vol. 73, 1976, pp. 465-495.

[12] Hussein, H. J., Capp, S. P., George, W. K.: Velocity measurements in a high-Reynolds-number,

momentum-conserving, axisymmetric, turbulent jet, Journal of Fluid Mechanics, Vol. 258, 1994, pp. 31-75.

[13] Delville, J., Bellin, S., Garm, J. H., Bonnet, J. P.: Analysis of Structures in a Turbulent, Plane Mixing Layer by Use of a Pseudo Flow Visualization Method Based on Hot-Wire Anemometry. In: Fernholz, H. H., Fiedler, H. E. (Eds.): Advances in Turbulence 2, Springer, 1989, pp. 251-256.

[14] Bradshaw, P., Ferriss, D. H., Atwell, N. P.: Calculation of boundary-layer development using the turbulent energy equation, Journal of Fluid Mechanics, Vol. 23, 1967, pp. 593-616.

[15] Wilcox, D.C.: Turbulence Modeling for CFD, DCW Industries, La Canada, CA, 3rd Ed., 2006.

[16] Jakirlic, S., Maduta, R.: On 'Steady' RANS Modeling for improved Prediction of Wall-bounded Separation, AIAA Paper 2014-0586, January 2014.

[17] Schatzman, D.M., Thomas, F.O.: An experimental investigation of an unsteady adverse pressure gradient turbulent boundary layer: embedded shear layer scaling, Journal of Fluid Mechanics, Vol. 814, 2017, pp- 592-642.

[18] Greenblatt, D., Paschal, K. B., Yao, C.-S., Harris, J., Schaeffler, N. W., Washburn, A. E.: A Separation Control CFD Validation Test Case, Part 1: Baseline and Steady Suction, AIAA Journal, Vol. 44, No. 12, 2006, pp. 2820-2830.

[19] Greenblatt, D., Paschal, K. B., Yao, C.-S., Harris, J.: A Separation Control CFD Validation Test Case, Part 2: Zero Efflux Oscillatory Blowing, AIAA Journal, Vol. 44, No. 12, 2006, pp. 2831-2845.

[20] Naughton, J. W., Viken, S. A., Greenblatt, D.: Skin-Friction Measurements on the NASA Hump Model, AIAA Journal, Vol. 44, No. 6, 2006, pp. 1255-1265.

[21] Schwamborn, D., Gerhold, T., and Heinrich, R.: The DLR TAU-Code: Recent Applications on Research and Industry, ECCOMAS, 2006.

[22] Rumsey, C.L.: Turbulence Modeling Resource, https://turbmodels.larc.nasa.gov/, retrieved May 10, 2019.

[23] Driver, D. M. and Seegmiller, H. L.: Features of a Reattaching Turbulent Shear Layer in Divergent Channel Flow, AIAA Journal, Vol. 23, No. 2, 1985, pp. 163-171.

[24] Menter, F.R.: Two-Equation Eddy-Viscosity Turbulence Models for Engineering Applications, AIAA Journal, Vol. 32 No. 8, 1994, pp. 1598-1605.

[25] Hanjalic, K. and Jakirlic, S.: Contribution Towards the Second-Moment Closure Modelling of Separating Turbulent Flows, Computers and Fluids, Vol. 27, No. 2, 1998, pp. 137-156.

[26] Yap, J. C.: Turbulent Heat and Momentum Transfer in Recirculating and Impinging Flows, PhD Thesis, University of Manchester, Faculty of Technology, 1987.

[27] Hanjalic, K. and Launder, B.: Modelling Turbulence in Engineering and the Environment, Cambridge University Press, New York, 2011.